Screening for Proteins Related to The Biosynthesis of Hispidin and Its Derivatives in *Phellinus Igniarius* Using iTRAQ Proteomic Analysis

Jinjing Guo
Ningxia medical university
Xiaoxi Liu
Ningxia medical university
Yuanjie Li
Ningxia medical university
Hongyan Ji
General hospital of Ningxia medical university
Cheng Liu
Ningxia Medical University
Li Zhou
Ningxia medical university
Yu Huang
Ningxia Medical University
Changcai Bai
Ningxia medical university
Zhibo Jiang
North Minzu university
Xiuli Wu (myjustmy@163.com)
Ningxia medical university

Research article

Keywords: Phellinus igniarius, Biosynthesis, Hispidin, iTRAQ, Proteomic

Posted Date: September 14th, 2020

DOI: https://doi.org/10.21203/rs.3.rs-72805/v1

Version of Record: A version of this preprint was published at BMC Microbiology on March 12th, 2021. See the published version at https://doi.org/10.1186/s12866-021-02134-0.

Abstract

Background: Hispidin (HIP) and its derivatives, a class of natural fungal metabolites, possess extremely complex and interesting chemical structures with extensive pharmacological activities. *Phellinus igniarius*, which is the most common sources of HIP, can be used as both medicine and food. The biosynthetic pasthway of HIP in *P. igniarius* is not yet clear and hence effective regulatory mechanism of HIP is absent.The purpose of this paper was to illustrate a biosynthesis system for hispidin and its derivatives at the protein level.

Results: We found that tricetolatone (TL) is a key biosynthetic precursor in the biosynthetic pathway of hispidin and that its addition led to increased production of hispidin and various hispidin derivatives. Based on the changes in the concentrations of precursors and intermediates, key timepoints in the biosynthetic process were identified. We used isobaric tags for relative and absolute quantification (iTRAQ) to study dynamic changes of related proteins *in vitro*. The 270 differentially expressed proteins were determined by GO enrichment analysis to be primarily related to energy metabolism, oxidative phosphorylation, and environmental stress responses after TL supplementation. The differentially expressed proteins were related to ATP synthase, NAD binding protein, oxidoreductase, and other elements associated with electron transfer and dehydrogenation reactions during the biosynthesis of hispidin and its derivatives. Multiple reaction monitoring (MRM) technology was used to selectively verify the iTRAQ results, leading us to screen 11 proteins that were predicted to be related to the biosynthesis pathways.

Conclution: These findings help to clarify the molecular mechanism of biosynthesis of hispidin and its derivatives and may serve as a foundation for future strategies to identify new hispidin derivatives.

Background

As a category of daily nutrient and medicine in Asian nations, edible and medicinal fungi have become an important source of biologically active components. *Phellinus igniarius* (DC.Ex Fr.) Quel, a wild macrofungi contains many bioactive compounds that have been reported to possess antibacterial, antioxidative, antitumor and antimutagenic activities, which have been widely used in China, Japan, and Korea for many years[1–3]. *P. igniarius* is rich in secondary metabolites with biological activities, such as polysaccharides, polyphenols, flavonoids and other species[4, 5]. A class of chemical compounds named Phelligridin from *P. igniarius* possess radical-scavenging activity and a broad pharmacological properties, such as Phelligridin D and Phelligridin G[6, 7]. According to their structure, it was postulated that phelligridins mediated by the fungal metabolite intermediate hispidin[8]. Hispidin (6-(3,4-dihydroxystyryl)-4-hydroxy-2-pyrone, HIP), is an important polyphenol found in *P. igniarius*. Hispidin is widely distributed in edible mushrooms and its value comes out, with many cases reported in the literature[9, 10]. Many studies have shown that HIP has pharmacological activities such as anti-oxidation[11], anti-inflammatory[12], anti-cancer[13], and antiallergic[14], among others. HIP is also an important luciferin precursor in some bioluminescent fungi and it can be applied in bioluminescent method for the analysis of substances[15, 16]. The present study demonstrates that 3 mg/g hispidin-enriched fungus mycelia has a very low order of toxicity, which supports its safety for human consumption[17]. Therefore, HIP has attracted quite a lot of attention in the fields of chemistry, pharmacy and microbiology[18–21].

Due to the limited and unstable supply of wild *P. igniarius*, artificial fermentation has caused the extensive concern in recent years.Significant recent research has focused on optimizing fermentation conditions with the goal of increasing the yield of HIP[17]. With the development of the sequencing technology, gene expression control at the transcriptional level was a possible regulation to determining compositon and facilitate industrial produce. The biosynthetic pathway is the prerequisite and foundation of genetically modified. However, biosynthetic pathway of HIP and its derivatives in *P. igniarius* has been the focus of extensive research but exact mechanism is still not understood. A previous study proposed the biosynthesis of HIP from Fig. 1. HIP formed by the condensation of 4-hydroxy-6-methyl-2-pyrone (TL) and one molecule of 3,4-dihydroxybenzoyl-SCoA (or 3,4-dihydroxybenzaldehyde) in *P. igniarius* fruit body[22]. This hypothesis has rarely been studied and verified, and the biosynthetic pathway of HIP has not been categorically confirmed.

This study investigated whether TL will be transformed into HIP in fermentation broth of P. igniarius. Moreover, the protein expression abundance was analyzed for the mycelium of P. igniarius following the TL feeding using the iTRAQ technology. The related proteins of HIP synthesis were identified. The analysis explored how these proteins participated in the responses to TL precursor feeding, and aimed at resolving the synthesis mechanisms of HIP at the proteomic level.

Results

Metabolic analysis method determination

The HPLC method was optimized to distinguish between HIP and other derivatives in order to analyze the ethyl acetate extracts. As seen in Fig. 2, the peak at 19.7 min was attributed to HIP, while 23.4 min was phelligridin D, and 9.6 min was TL. To determine that the peaks at 19.7 min and 23.4 min were indeed HIP and phelligridin D, the chemical structures of two purified compounds **A** and **B** were elucidated by NMR spectra and HRESIMS (see Fig. S1-9).

Compound **A** was obtained as a light-yellow powder. Its quasi-molecular ion peak, observed at *m/z* 245.0453 (cal. 245.0450) $[M - H]^-$ by HRESIMS and NMR data, showed the molecular formula as $C_{13}H_{10}O_5$. The ^{1}H-NMR spectrum of **A** in CH_3OD (see Fig. S3) displayed resonances in pairs attributable to two analogous compounds with a content ratio of 3:2. Through detailed analysis, the difference was focused on the *cis* and *trans* double bonds and some changes in chemical shift. The resonances were ascribed to two ABX spin coupling systems of 1,3,4-trisubstituted phenyl moiety at d_H 6.95 (dd, J = 2.0, 8.0 Hz), 6.77 (d, J = 8.0 Hz), 7.03 (d, J = 2.0 Hz), and d_H 6.80 (dd, J = 2.0, 8.0 Hz), 6.73 (d, J = 8.0 Hz), 6.98 (d, J = 2.0 Hz), a *trans*-disubstituted and a *cis*-disubstituted double bond at d_H 7.31 (d, J = 16.0 Hz), 6.60 (d, J = 16.0 Hz), and 6.72 (d, J = 12.8 Hz), 5.98 (d, J = 12.8 Hz). The ^{13}C-NMR spectrum of **A** gave two sets of 12 sp^2 carbon resonances. Compared with the peak position of standards in HPLC and the data from HRESIMS, the compound was speculated to be a combination of *trans*-hispidin and *cis*-hispidin (see Fig. S1), which was also confirmed by 2D NMR. Analysis of gHSQC spectroscopic data of A furnished assignments of the proton-bearing carbon and corresponding proton resonances in the NMR spectra (Table 1). Although the signals of H_3 and C_3 disappeared in NMR, the visible long-range heteronuclear correlations in the HMBC of *trans*-hispidin for H-5/C-3 (~90 ppm, see Fig. S7) and the data in the literature[11, 23] supported the prior findings. Regardless of whether it is *trans* or *cis*, hispidin is a crucial intermediate of phelligridins[22].

Compound **B** was obtained as a yellow powder. Its quasi-molecular ion peak, found at *m/z* 379.0466 (cal. 379.0454) $[M - H]^-$ by HRESIMS, gave a molecular formula of $C_{20}H_{12}O_8$. Compound **B** was identified as phelligridin D by comparing with standards and data from ^{1}H-NMR spectra (see Fig. S9)[22].

The concentration dynamic changes of TL and HIP

Compared to the negative control that was not given TL, the contents of HIP were increased five-fold three days after the addition of TL, and the content of TL gradually decreased (Fig. 3), suggesting that TL participates in the biosynthesis of HIP. Interesting, the content of TL and hispidin from 8 to 16 hours after TL feeding were contrary to the general trends observed over the longer time period, suggesting that the strain was in the logarithmic phase of growth through this period. Hispidin content rose sharply over the course of 16-64 h from < 5 mg/L at 16 h to 44.38 mg/L at 64 h, and TL rapidly (during the first 128 h after addition, the concentration of TL declined from 423.61 mg/L to 50.44 mg/L), indicating that TL may be consumed to synthesize hispidin. After 64 h, the concentration of HIP began to decline, presumably due to the synthesis of other derivatives.

iTRAQ protein analysis

Herein, the expression of different types of proteins by *P. igniarius* fed with either TL-supplemented or normal media were compared by iTRAQ analysis. A total of 339,985 spectrums were filtered by 1% FDR, which led to the identification of 5,630 peptides and 1,880 proteins (Fig. 4). These results indicated that iTRAQ had higher sensitivity and provided more comprehensive information than other techniques in the analysis of these fungal proteins. The molecular weights of the identified proteins were widely distributed, mostly falling between 10 and 70 kDa.There were 710 proteins with molecular weights over 100 kDa , and 552 between 20-30 kDa, 794 proteins between 30-40 kDa, and 543 between 40-50 kDa (Fig. 5A and 5B). Protein coverage analysis showed that the numerical value from 0% to 100% was gradually declined. There were 966 proteins with specific more than 11 peptide segments. The number of specific spectra is shown in Fig. 5C. The number distribution of specific peptide segments is shown in Fig. 5D. The specific peptide segments, was very really reflected the reliability of the results.

Analysis of the difference expression of proteins (DEPs)

Screening of DEPs was carried out to determine which proteins were expressed with a fold change > 1.5 and a Q value < 0.05. We identified 615 DEPs in the TLPF32h group, including 385 up-regulated proteins and 230 down-regulated proteins. There were 907

DEPs in the control group compared with TLPF128h, including 249 up-regulated proteins and 458 down-regulated proteins. As can be seen in Fig. 6, up-regulation of proteins was more common after the addition of TL, but the number of down-regulated proteins was higher in the TLPF128h group compared to the TLPF32h group.

Gene ontology (GO) is an important element of bioinformatics research that aims to unify analyses of gene expression and gene attributes of all species. GO annotation analysis showed that 297 DEPs in the TLPF32h group and control group were annotated as belonging to 35 functional groups (Fig. 7). Briefly, the DEPs were found to be mainly involved in cellular processes (38.05%) and metabolic processes (34.34%). Among the cell components, DEPs were mainly concentrated in cells (39.73%) and cell parts (39.06%). In terms of molecular function, DEPs were mainly involved in catalytic activity (55.56%) and binding activity (46.46%).

These results indicated that TL-reactive proteins may be primarily involved in stress responses, chemical stimulation responses, primary metabolic processes, cell responses, and other related functions. We might expect that when *P. igniarius* experiences changing environmental stimuli, the defense system would immediately respond, increasing metabolic activity, producing defensive substances, and enhancing the activity of various enzymes to promote defense.

In KEGG pathway enrichment analysis, a total of total 82 DEPs were matched with the KEGG pathway database using Blast_v2.2.26 software. Compared with the control group (Fig. 8), 265 DEPs were labeled as 52 KEGG pathways, and metabolic pathways (ko01100, 77 DEPs) were the primary pathways that were enriched. Indeed, the DEPs were clearly concentrated in metabolic pathways and oxidative phosphorylation, and most of these were up-regulated. Thus, it appears that TL supplementation accelerates *P. igniarius* metabolism and produces oxidative stress. The other DEPs that were identified were mainly related to secondary metabolites and ribosomal protein biosynthesis in the TLPF128h group. Ribosomal proteins represent a common type of RNA-binding protein, which mainly participate in protein translation, post-translational modification, or protein folding. Because we found that the ribosomal protein pathway was down-regulated, we hypothesize that the synthesis of new protein would be slowed. Compared with the TLPF32h group, metabolic processes and ribosomal proteins were the differentially regulated main pathways in the TLPF128h group. Most of the differentially expressed proteins (DEPs) in the 128h group were down-regulated relative to 32h, suggesting that the metabolic rate decreased over time.

Selective verification of iTRAQ data by mass spectrometry multi-reaction monitoring technology (MRM)

In light of the above protein analysis results, 15 candidate DEPs related to the TL reaction were selected to establish MRM method. Of the 15 target proteins, 11 had MS/MS spectra and unique peptide(s). Therefore, those 11 DEPs were detected and quantified by MRM (Table 2). The results showed that the expression levels of DEP and iTRAQ were in almost direct agreement with each other.

Discussion

At present, genomic mining and functional determination are commonly used in the study of the mechanism of fungal composition biosynthesis. The synthetic genes and regulatory mechanisms of some fungal products have been elucidated in detail, such as monacolin K[24] and griseofulvin. Hispidin and its derivatives are active constituents of edible fungi[25]. Proteomic analysis is considered to be an important for mechanistic studies because of the uncertainties involved with genome sequencing and biosynthetic pathways of compounds. This method was utilized in the early study of the biosynthesis of aflatoxin, and the hypothesis of the biosynthesis mechanism was confirmed by feeding the intermediate versicolorin A and using LC-MS/MS to analyze the resulting proteins[26].

In this study, the proteins involved in the biosynthesis of secondary metabolites were identified by iTRAQ method for the first time, and a large number of DEPs were detected in *P. igniarius* after supplementation with the precursor molecule TL. In addition, there were 270 DEPs that were mainly separated into groups, including energy metabolism, oxidative phosphorylation, and environmental stress responses. These proteins may provide a new perspective for the study of the biosynthesis of hispidin and its derivatives. Comparative analyses showed that DEPs found after TL feeding were mainly involved in cell processes, metabolic processes, located in cells or cell parts, catalytic activities, and binding functions.

Comparing the proteomic changes after TL supplementation

By noticing the dynamic changes in concentration of HIP, TL supplementation led to significant improvementof HIP production. KEGG pathway enrichment analysis of three group indicated that DEPs of TLPF32h vs control group most closely associated with metabolic

pathway(Figure 8). Almost all proteins had high expression levels that participated in oxidative phosphorylation. The proton pump F-ATPase is an ATP synthase, which plays an important role in energy transduction in most species. Further, the F-ATPase helps maintain the pH of the cytoplasm by secreting protons, and F-ATPase inhibitors reduce the acid resistance of bacteria[27]. In this study, a large number of F-ATPase were up-regulated after TL feeding. The enhancement of ATP synthase, consistent with increased expression of proteins related to oxidative phosphorylation, could increase the ATP supply to the biosynthesis of HIP. Consistently,proteomic analysis showed that NADH dehydrogenase related energy production were also up-regulated in *P.igiarius*. NADH dehydrogenase is the major element of respiratory chain complex I, Electrons mainly move from NADH to the mitochondrial respiratory chain. NADH dehydrogenase is a small protein (<10 kDa) and relatively simple in structure[28]. Its sub-structures and functional model have been well established. In this study, several complex I subunits were up-regulated to produce more protons, which could promote ATP synthesis. That is to say, in *P. igniarius*, increased synthesis of ATP may play a central role in the differential expression seen after supplementation with TL. This ATP-related enzyme were down-regulated at KEGG pathway enrichment analysis of TLPF128h vs TLPF32h group. The inexistence of riboflavin, thiamine, glutathione, cysteine and methionine, snd selenocompound metabolism at TLPF128h vs TLPF32h group showed mycelium metabolism basically return to normal. It is worth noting that protein of ribosome is significantly down-regulated in TLPF128h. This suggest that synthesis of protein was decreased at that time.

Environmental stress may lead to the accumulation of HIPs

Whereas the regulation mechanism of macrofungi is unclear because of the complexity of the physiological process and complex genomes. In the past years, development of proteomics provided insights into a systematic understanding of the filamentous fungi and yeast at the molecular level in response to environmental change, such as response of *Flammulina velutipes* to cold and light stress[29]. Among the 270 DEPs, some were stress proteins produced by organisms in response to environmental changes. For example, cysteine proteases respond to biological and abiotic stressors in the external environment. They not only participate in the regulation of transcription factors, but also process proteins[30]. Glutathione S-transferases, which are mainly found in the cytoplasm, are multifunctional supergene family proteins. Fungal glutathione S-transferases have a variety of structures and functions, regulate the growth and development of organisms, and protect the enzyme system from environmental stress[31]. Heat shock protein (HSP) is another type of stress protein produced by organisms in response to environmental changes. Recent studies have shown that HSPs are ubiquitous in prokaryotes and eukaryotes. HSPs are a type of newly synthesized proteins that help to maintain proper protein folding, promote the transmembrane transport of protein molecules, and promote the recovery or degradation of damaged proteins. In emergencies, the increase concentration of oxygen free radicals in cells affects the permeability and fluidity of cell membranes, thus affecting the normal metabolism of cells and organelles. In order to promote the hydrolysis of ATP, HSPs activate protein kinase C, thereby reducing the damage caused by oxygen free radicals. Recent research showed that pyruvate accumulation is one of protection mechanism against stress condition in fungus[32]. In this study, our data showed that pyruvate dehydrogenase and dihydrolipoyllysine-residue acetyltransferase content were increased, probably because that pyruvate accumulation(Figure 9). These proteins play an important role in the defense response and were up-regulated in TLPF32h. Our previous studies showed that there was trace hispidin and hispidin derivatives in the fermentation broth of *P. igniarius*, found at concentrations too low to be separated and extracted. However, the compounds can be extracted from the fruiting bodies of wild fungi. The data of stress proteins indicated that TL feeding caused a stress reaction in *P. igniarius* mycelium. The content of HIP tended to increase in the meantime. Therefore, we speculate that the hispidin metabolic pathway in *P. igniarius* may be related to the accumulation of secondary metabolites in stressful environments.

Biosynthesis pathway of HIPs

The biosynthesis pathway of HIP were inferred that the cinnamate pathway for the metabolism of phenylalanine is origin of HIP synthesis as far back as 1973[33]. Recent research revealed that HIP is precursor of luciferin 3-hydroxyhispidin[34]. It has been found that luminescence of luminous fungal fruiting body extract enhance gradually by the addition of hispidin biosynthetic components, namely caffeic acid, ATP and malonyl-CoA[35]. Another theory, that HIP is condensated by TL and 3,4-dihydroxybenzaldehyde based the chemical structure of compounds which isolated from the fungus fruiting body[22]. Biogenesis of many HIP derivatives prompted speculation that it is biogenerated by the condensation of HIP, which is a process that could be catalyzed by peroxidase[36]. The synthesis mechanism of HIP and other complex derivatives is however not specific.

TL is a common small molecule polyketone precursor compound that participates in the biosynthesis of HIPs. Expression of the protein GME4094_g which is polyketide synthase down-regulated in TLPF32h and no longer up-regulated in TLPF128h (Table 3). In the synthesis process of HIP, dehydrogenase is needed. Dehydrogenases GME1855_g, GME4242_g, GME4316_g, and GME9582_g are

essential in the HIP synthesis pathway, and they were increased during the HIP production period. A series of enzymes related to the biosynthesis of HIPs are listed in Table 3. In addition, some oxygenase (Table 4) appeared to play a role in the synthesis of HIP's structural derivatives (such as phelligridin D, Fig.9). In this process, phenolic compounds are oxidized to benzoquinones that stimulate free radical transfer and then form a variety of compounds with novel chemical skeletons. With the elucidation of secondary metabolites biosynthesis pathway and study regulation of its biosynthesis, it has become possible to regulate its biosynthesis via genetic engineering.

Conclusion

In this study, a new synthetic pathway of hispidin was analyzed and validated by the precursor feeding method. The DEPs of *P. igniarius* after TL feeding were analyzed using the iTRAQ technique, and DEPs involved in the biosynthesis of hispidin and its derivatives were subsequently screened. The synthesis of hispidin and its derivatives may be related to a large number of oxidoreductases and dehydrogenases and to stress response systems. According to the results of differential proteomic analyses and previous data, it appears that TL affects the biosynthesis of hispidin through reactive oxygen species scavenging, signaling pathways, secondary metabolite synthesis, and other reactions. This work sought to provide mechanistic clarification for the biosynthetic pathways important for the production of hispidin and its derivatives through analysis of whole gene sequences, functional gene annotations, and prediction of secondary metabolite synthesis gene clustering, combined with analysis of DEPs from iTRAQ results. Further research should focus on further studies of the biosynthetic gene cluster and synthetase of hispidin.

Methods

Materials

P. igniarius (CGMCC 5.95) was purchased from the China Microbial Preservation Center (Beijing, China) and was cultured in modified Martin medium (MMM), including 5 g/L peptone, 1 g/L K_2HPO_3, 2 g/L yeast extract, 20 g/L glucose, 20 g/L agar, pH 6.2-6.5. The culture medium was sterilized by autoclave at 121 ℃ for 30 min. The strain was stored at 4 ℃ for further studies.

HPLC detection of metabolites by precursor feeding

P. igniarius was cultured in MMM medium for seven days at 28 ℃. An agar patch (1 cm × 1 cm) was added into a 250 mL conical bottle containing 150 mL liquid medium (the above MMM without agar). The culture conditions were 28 °C, 180 rpm. Then, 15 days later, the TL, which was dissolved in double distilled water, was added into the fermentation liquor at a final concentration of ~0.1 mg/mL. The co-culture was then allowed to grow for another 9 days under the same conditions. Samples (2.0 mL) were taken at 1, 3, 5, 7, and 9 days after the addition of TL, and were extracted by EtOAc (3 × 2.0 mL). The organic layer was removed by volatilization and the residue was dissolved in 2 mL methanol for HPLC detection. HPLC was conducted using Agilent 1220 Infinity II equipment with Agilent Eclipse XDB-C18 (4.6 mm × 250 mm, 5 μm) as the separation column. Two-phase gradient elution methods were used in this work including 0.2% formic acid (an aqueous solution) as phase A, and MeOH as phase B. The MeOH in phase B was gradually increased from 40% (V/V) to 80% (V/V) over 25 min. The spectra were recorded by a DAD detector at 380 nm. The flow velocity was set to 1 mL/min, and the injection volume was 10 μL.

Separation and identification of metabolites

A 5,000 mL scale-up of *P. igniarius* was cultured according to the above-mentioned fermentation conditions. After the 0.1 mg/mL TL was added, the co-culture was grown for another 3 days. The filtrate of the fermentation broth was concentrated to 500 mL and partitioned with EtOAc (3 × 500 mL). The EtOAc extract was then evaporated under reduced pressure to yield 290 mg of residue, which was subjected to Sephadex LH-20 column chromatography, eluted with petrol-$CHCl_3$-MeOH (5:4:1) to produce five fractions (A-E). Fraction B was purified through reverse-phase preparative HPLC using a mobile phase of MeOH-H_2O (45:55) to afford compound **A** (25.5 mg). Fraction D was separated by preparative RP-HPLC using MeOH-H_2O (62:38) to afford compound **B** (7.0 mg). The structures of the target compounds were identified by 1D, 2D NMR and HRESIMS analysis. 1D- and 2D-NMR spectra were obtained at 400 MHz for ^1H and 100 MHz for ^{13}C, respectively, on Bluker 400 MHz spectrometers in methanol-d_4 with solvent peaks used as references. HRESIMS data were measured using an Agilent 1290 Infinity II Accurate Mass Q-ToF LC/MS spectrometer.

Determination of HIP yield by external standard method

The concentrations of HIP and TL were determined by HPLC with an external standard at the wavelength of 254 nm, and a 20-80% methanol gradient was used for elution. the concentration points for the HIP standard curve were 1.0, 0.5, 0.25, 0.125, 0.0625 and 0.03125 mg/mL, and the concentrations for the TL standard curve were 8, 4, 2, 1, 0.5, and 0.25 mg/mL. The linear standard equation was obtained by using the linear least square method. As in the previous methods description, *P. igniarius* was cultured in MMM liquid medium for 15 days and then fed TL at a final concentration of 0.1 mg/mL. Fermentation broth samples were taken at 0 h, 1 h, 2 h, 4 h, 8 h, 32 h, 64 h, and 128 h after the addition of TL into the fermentation system, and then the samples were extracted with ethyl acetate and analyzed by HPLC.

Protein extraction and enzymatic hydrolysis

A 5 mm magnetic bead and 25 μL of lysis buffer were added to 5 mg mycelium samples. The final concentrations of PMSF and EDTA were 1 mM and 2 mM, respectively. The mycelium samples were allowed to rest for 5 minutes after the eddy oscillation, and the final concentration of DTT was 10 mM. The supernatant was collected by centrifugation at 4 ℃ for 20 min after 2 min oscillation with a tissue abrasive apparatus. The supernatant was treated with 10 mM DTT for 1 hour in a water bath at 56 ℃. After coming back down to room temperature, IAM was added at a final concentration of 55 mM, and then the sample was kept in the dark for 45 minutes. The supernatant was precooled with 5× volume of acetone, precipitated at -20 ℃ for 2 h, and was centrifuged at 9000 × g, 4 ℃ for 20 min. The addition of acetone was repeated three times, followed each time by centrifugation and discarding the supernatant until the supernatant was colorless. 25 μL of lysis buffer was added into the precipitation mixture. After 5 minutes of ultrasonication in an ice bath, the supernatant was centrifuged at 9000 × g, 4 ℃ for 20 min.

iTRAQ marker and peptide segment separation

First, 100 μg protein solution was extracted from each sample, and the trypsin enzyme was added in the ratio of protein:enzyme of 40:1. The enzyme was hydrolyzed for 4 hours at 37 ℃, at which point trypsin was again added (the same amount), and the mixture was continuously hydrolyzed for another 8 hours. The resulting enzymatically generated peptides were desalted using a Strata X column and then vacuum-dried.

Eight groups of iTRAQ labeling reagents (113, 114, 115, 116, 117, 118, 119, 121) were selected. Then, 50 μL isopropanol were added to each tube at 25 ℃, and the mixture was centrifuged after swirl oscillation. The supernatants were transferred to another clean sample tube along with the enzymatic peptides in 0.5 M TEAB. The different peptide fragments were labeled with their respective peptide's labels.

The above samples were separated by liquid phase chromatography with a LC-20AB system (Shimadzu, Japan), and the separation column used was a Gemini C18 column (5 μm, 4.6 × 250 mm). The above dried samples were re-dissolved with phase A (5% ACN, pH 9.8), and the flow rate gradient was set as: 5% mobile phase B (95% ACN, pH 9.8) for 10 minutes, 5-35% mobile phase B for 40 minutes, 35-95% mobile phase B for 3 minutes, and 5% mobile phase B for 10 minutes, at rate of 1.0×10^{-3} L/min. The detection wavelength used was 214 nm. The fractions were collected once per minute, and the sample components were merged by chromatographic elution peaks to yield a total of 20 fractions. Those 20 fractions were frozen and concentrated each to the same volume of 1.0 mL.

LC-MS/MS analysis

After centrifugation for 10 minutes, the supernatant samples were separated using LC-20AD nanoflow liquid chromatography. A trap column was used to concentrate protein and remove salts. It was connected with a self-assembled C18 column (75 micron inner diameter, 3.6 micron column diameter, 15 cm column length) in series. The flow rate was set to 300 nL/min. Separation was carried out using the following gradients:

(1) 0-8 minutes, 5% mobile phase B (98% acetonitrile aqueous solution containing 0.1% formic acid (FA));

(2) 8-43 minutes, 8-35% mobile phase B gradient;

(3) 43-48 minutes, 35-60% mobile phase B gradient;

(4) 48-50 minutes, 60-80% mobile phase B gradient;

(5) 50-55 minutes, equivalent 80% mobile phase B;

(6) 55-65 minutes, equivalent 5% mobile phase B.

After ionization from a nano ESI source, the peptide segments were analyzed by high resolution liquid chromatography-mass spectrometry (HR-LC-MS) TripleTOF 5600. Using Proteome Discoverer, a Thermo science tool, the original mass spectrometry file was converted into a MGF format file containing the information of secondary mass spectrometry (MS/MS) spectra, in which "BEGIN IONS" and "END IONS" were the starting and ending positions of each spectrum. The UniProt protein database was used to identify the proteins. The MGF file and protein database were searched to obtain the final protein identification results using the Mascot 2.3.02 identification software.

iTRAQ data analysis

iTRAQ data were quantified by IQuant software. The spectra and the list of peptide segments were filtered by 1% FDR (PSM-level FDR < 0.01) to identify significant results. According to the parsimony principle, the peptide segments were used to assemble proteins and produce a series of proteomes. In order to control the false positive rate of proteins, the process was again filtered at the protein level with 1% FDR (Protein-level FDR < 0.01). Quant's workflow included the following steps: protein filtering, purity correction of report group labels, normalization of quantitative values, complementation of missing values, calculation of quantitative values of proteins, statistical analysis, and display of final results.

Bioinformatic analysis

In this study, three sets of experiments including Control, TLPF32h, TLPF128h, and three sets of comparisons of TLPF32h /control, TLPF128h/control, TLPF128h/TLPF32h were conducted. The differentially expressed proteins (DEPs) were screened on the basis of a fold change > 1.5 and $P < 0.05$.

In the GO enrichment analysis of DEPs, the GO entries with significant enrichment were identified by hypergeometric test, compared with all identified proteins as background. The principle of Pathway enrichment analysis was similar. The hypergeometric test formula was as follows:

$$P = 1 - \sum_{i=0}^{m-1} \frac{\binom{M}{i}\binom{N-M}{n-i}}{\binom{N}{n}}$$

N: The number of GO entries matched in all identified proteins; n: the number of GO entries matched in DEPs; M: one of the GO entries matched in all identified proteins; m: one of the GO entries matched in DEPs. DEPs were determined to be significantly enriched in the GO entry if the P value of the hypergeometric test was less than 0.05.

Validation of MRM Technology

According to the results of iTRAQ data, differentially expressed proteins were screened and selected for MRM validation. Each sample was treated with 100 μg protein solution. Trypsin enzyme was added at a ratio of protein:enzyme of 40:1, with a total amount of 2.5 μg of trypsin enzyme, and enzymatic hydrolysis was carried out at 37 ℃ for 4 hours. Trypsin was added one more time at the same ratio, and the enzymatic hydrolysis was continued at 37 ℃ for another 8 hours. The enzymatic peptides were desalted using a Strata X column and then vacuum-dried.

The samples were scanned with a HPLC-TripleTOF 5600 mass spectrometer, and the resulting data were searched by Mascot v2.3 using the Fungi protein database (11,243 sequences) added to the internal standard peptide sequence. The DAT files were imported into Skyline software to establish the atlas library (credibility > 0.95). Skyline software was used to select target peptide segments under the following conditions:

(1) The peptide segments had matched second-order ions.

(2) The length of the peptide segments were between 5-40 amino acids.

(3) The peptide segment was the only one for the target protein.

(4) The cysteine in the peptide segment was modified to carbamidomethyl.

(5) There was no variable modification of the peptide segment.

(6) No methionine was found in the peptide segment.

(7) There was no missing cut of the peptide segment.

Transition selection set was determined as follows:

(1) The fragment ions were B and Y ions;

(2) The parent ion charges were 2,3,4;

(3) The charges of fragment ions were 1,2;

(4) Debris ion charge-mass ratio < 1,250 (four-stage rod scanning range);

(5) The number of transitions was 6.

Validation of MRM method

Skyline set up the MRM method and output it to the QTRAP 5500 mass spectrometer for MRM scanning verification. The success of MRM mass spectrometry for target proteins depended on the validation results, which must conform to:

(1) There were co-elution peaks in transitions with different peptide segments.

(2) The chromatographic peak area intensity of transitions with different peptide segments was correlated with the fragmentation intensity of spectral data.

(3) The retention time of the peptide segments in MR and full-spectrum scans was good.

MRM Mass Spectrometry Detection

The peptide fragments were separated by liquid phase and entered into the QTRAP 5500 tandem mass spectrometer. The ion source was Nanospray Illsource. In data acquisition, the instrument parameters are set as follows: spray voltage was 2,400V, spray gas was 23. With MRM scanning mode, the resolution of Q1 and Q3 was set to Unit mode.

Data analysis

Each transition signal of the target protein was normalized to the signal of beta-galactosidase. After normalized intensity, a linear mixed model integrated with the MSstats tool was used to quantify the target protein in the sample. This model gave the ratio of protein in the comparison group and the adjusted p-value. The corrected P value reflected the false positive rate of the original statistical test (Benjamin and Hochberg). If the difference in final target protein concentration was at least 1.5-fold with $P < 0.05$ (false positive < 0.05), the protein was considered to be significantly differentially expressed.

Declarations

Ethics approval and consent to participate

Not applicable.

Consent for publication

Not applicable.

Availability of data and materials

All data generated or analyzed during this study are included in this article.

Competing interests

The authors declare that they have no competing interests

Funding

The project was financially supported by the National Natural Science Foundation of China (NNSFC; grand nos: 81960643, 81560567) and Key R&D projects in Ningxia province (grant nos: 2020BFG02006).

Author's contributions

WXL and JZB responsible for the overall arrangements for the study. GJJ and LXX made substantial contributions to the experimental operation and data acquisition. GJJ drafted the manuscript and JHY revised it critically for important intellectual content. LC , ZL, HY and BCC analyzed and interpreted the data. All authors read and approved the final manuscript.

Acknowledgements

Not applicable

Supplementary material

Figures S1-9, MS, 1D and 2D NMR spectra of compounds **A** and **B**. This material is available free of charge via the Internet at http://www.sciencedirect.com.

References

1. Wang Y, Shang XY, Wang SJ, Mo SY, Li S, Yang YC, Ye F, Shi JG, He L: **Structures, biogenesis, and biological activities of pyrano[4,3-c]isochromen-4-one derivatives from the Fungus Phellinus igniarius**. *J Nat Prod* 2007, **70**(2):296-299.
2. Zhang H, Ma H, Liu W, Pei J, Wang Z, Zhou H, Yan J: **Ultrasound enhanced production and antioxidant activity of polysaccharides from mycelial fermentation of Phellinus igniarius**. *Carbohydr Polym* 2014, **113**:380-387.
3. Konno S, Chu K, Feuer N, Phillips J, Choudhury M: **Potent Anticancer Effects of Bioactive Mushroom Extracts (Phellinus linteus) on a Variety of Human Cancer Cells**. *J Clin Med Res* 2015, **7**(2):76-82.
4. Gao W, Wang W, Sun W, Wang M, Zhang N, Yu S: **Antitumor and immunomodulating activities of six Phellinus igniarius polysaccharides of different origins**. *Exp Ther Med* 2017, **14**(5):4627-4632.
5. Lee MS, Hwang BS, Lee IK, Seo GS, Yun BS: **Chemical Constituents of the Culture Broth of Phellinus linteus and Their Antioxidant Activity**. *Mycobiology* 2015, **43**(1):43-48.
6. Kim JE, Takanche JS, Yun BS, Yi HK: **Anti-inflammatory character of Phelligridin D modulates periodontal regeneration in lipopolysaccharide-induced human periodontal ligament cells**. *J Periodontal Res* 2018, **53**(5):816-824.
7. Kim JY, Kim DW, Hwang BS, Woo EE, Lee YJ, Jeong KW, Lee IK, Yun BS: **Neuraminidase Inhibitors from the Fruiting Body of Phellinus igniarius**. *Mycobiology* 2016, **44**(2):117-120.
8. Wang Y, Mo SY, Wang SJ, Li S, Yang YC, Shi JG: **A unique highly oxygenated pyrano[4,3-c][2]benzopyran-1,6-dione derivative with antioxidant and cytotoxic activities from the fungus Phellinus igniarius**. *Org Lett* 2005, **7**(9):1675-1678.
9. Zan LF, Bao HY, Bau T, Li Y: **A New Antioxidant Pyrano[4,3-c][2]benzopyran-1,6-dione Derivative from the Medicinal Mushroom Fomitiporia ellipsoidea**. *Natural Product Communications* 2015, **10**(2):315-316.
10. Hwang BS, Lee IK, Choi HJ, Yun BS: **Anti-influenza activities of polyphenols from the medicinal mushroom Phellinus baumii**. *Bioorg Med Chem Lett* 2015, **25**(16):3256-3260.
11. Park IH, Chung SK, Lee KB, Yoo YC, Kim SK, Kim GS, Song KS: **An antioxidant hispidin from the mycelial cultures of Phellinus linteus**. *Arch Pharm Res* 2004, **27**(6):615-618.
12. Shao HJ, Jeong JB, Kim KJ, Lee SH: **Anti-inflammatory activity of mushroom-derived hispidin through blocking of NF-B activation**. *J Sci Food Agr* 2015, **95**(12):2482-2486.

13. Lim JH, Lee YM, Park SR, Kim DH, Lim BO: **Anticancer Activity of Hispidin via Reactive Oxygen Species-mediated Apoptosis in Colon Cancer Cells**. *Anticancer Research* 2014, **34**(8):4087-4093.
14. Tamrakar S, Fukami K, Parajuli GP, Shimizu K: **Antiallergic Activity of the Wild Mushrooms of Nepal and the Pure Compound Hispidin**. *Journal of Medicinal Food* 2019, **22**(2):225-227.
15. Purtov KV, Petushkov VN, Rodionova NS, Gitelson JI: **Why does the bioluminescent fungus Armillaria mellea have luminous mycelium but nonluminous fruiting body?***Dokl Biochem Biophys* 2017, **474**(1):217-219.
16. Puzyr AP, Medvedeva SE, Burov AE, Zernov YP, Bondar VS: **Detection of Hispidin by a Luminescent System from Basidiomycete Armillaria borealis**. *Dokl Biochem Biophys* 2018, **480**(1):173-176.
17. Li IC, Chen CC, Sheu S, Huang IH, Chen CC: **Optimized production and safety evaluation of hispidin-enriched Sanghuangporus sanghuang mycelia**. *Food Sci Nutr* 2020, **8**(4):1864-1873.
18. Grundemann C, Arnhold M, Meier S, Backer C, Garcia-Kaufer M, Grunewald F, Steinborn C, Klemd AM, Wille R, Huber R *et al*: **Effects of Inonotus hispidus Extracts and Compounds on Human Immunocompetent Cells**. *Planta Med* 2016, **82**(15):1359-1367.
19. Kim HG, Yoon DH, Lee WH, Han SK, Shrestha B, Kim CH, Lim MH, Chang W, Lim S, Choi S *et al*: **Phellinus linteus inhibits inflammatory mediators by suppressing redox-based NF-kappaB and MAPKs activation in lipopolysaccharide-induced RAW 264.7 macrophage**. *J Ethnopharmacol* 2007, **114**(3):307-315.
20. Lv LX, Zhou ZX, Zhou Z, Zhang LJ, Yan R, Zhao Z, Yang LY, Bian XY, Jiang HY, Li YD *et al*: **Hispidin induces autophagic and necrotic death in SGC-7901 gastric cancer cells through lysosomal membrane permeabilization by inhibiting tubulin polymerization**. *Oncotarget* 2017, **8**(16):26992-27006.
21. Kim DE, Kim B, Shin HS, Kwon HJ, Park ES: **The protective effect of hispidin against hydrogen peroxide-induced apoptosis in H9c2 cardiomyoblast cells through Akt/GSK-3 beta and ERK1/2 signaling pathway**. *Experimental Cell Research* 2014, **327**(2):264-275.
22. Mo S, Wang S, Zhou G, Yang Y, Li Y, Chen X, Shi J: **Phelligridins C-F: cytotoxic pyrano[4,3-c][2]benzopyran-1,6-dione and furo[3,2-c]pyran-4-one derivatives from the fungus Phellinus igniarius**. *J Nat Prod* 2004, **67**(5):823-828.
23. Zan LF, Qin JC, Zhang YM, Yao YH, Bao HY, Li X: **Antioxidant Hispidin Derivatives from Medicinal Mushroom Inonotus hispidus**. *Chem Pharm Bull* 2011, **59**(6):770-772.
24. Zhang C, Liang J, Yang L, Sun B, Wang C: **De Novo RNA Sequencing and Transcriptome Analysis of Monascus purpureus and Analysis of Key Genes Involved in Monacolin K Biosynthesis**. *PLoS One* 2017, **12**(1):e0170149.
25. Han JJ, Bao L, He LW, Zhang XQ, Yang XL, Li SJ, Yao YJ, Liu HW: **Phaeolschidins A-E, five hispidin derivatives with antioxidant activity from the fruiting body of Phaeolus schweinitzii collected in the Tibetan Plateau**. *J Nat Prod* 2013, **76**(8):1448-1453.
26. Linz JE, Chanda A, Hong SY, Whitten DA, Wilkerson C, Roze LV: **Proteomic and biochemical evidence support a role for transport vesicles and endosomes in stress response and secondary metabolism in Aspergillus parasiticus**. *J Proteome Res* 2012, **11**(2):767-775.
27. Sekiya M, Izumisawa S, Iwamoto-Kihara A, Fan Y, Shimoyama Y, Sasaki M, Nakanishi-Matsui M: **Proton-pumping F-ATPase plays an important role in Streptococcus mutans under acidic conditions**. *Arch Biochem Biophys* 2019, **666**:46-51.
28. Yagi T, Matsuno-Yagi A: **The proton-translocating NADH-quinone oxidoreductase in the respiratory chain: the secret unlocked**. *Biochemistry* 2003, **42**(8):2266-2274.
29. Liu JY, Chang MC, Meng JL, Feng CP, Wang Y: **A Comparative Proteome Approach Reveals Metabolic Changes Associated with Flammulina velutipes Mycelia in Response to Cold and Light Stress**. *J Agr Food Chem* 2018, **66**(14):3716-3725.
30. Wang W, Zhao P, Zhou XM, Xiong HX, Sun MX: **Genome-wide identification and characterization of cystatin family genes in rice (Oryza sativa L.)**. *Plant Cell Rep* 2015, **34**(9):1579-1592.
31. Shen M, Zhao DK, Qiao Q, Liu L, Wang JL, Cao GH, Li T, Zhao ZW: **Identification of glutathione S-transferase (GST) genes from a dark septate endophytic fungus (Exophiala pisciphila) and their expression patterns under varied metals stress**. *PLoS One* 2015, **10**(4):e0123418.
32. Zhang X, Leger RJS, Fang WG: **Stress-induced pyruvate accumulation contributes to cross protection in a fungus**. *Environ Microbiol* 2018, **20**(3):1158-1169.
33. Nambudiri AM, Vance CP, Towers GH: **Effect of light on enzymes of phenylpropanoid metabolism and hispidin biosynthesis in Polyporus hispidus**. *Biochem J* 1973, **134**(4):891-897.

34. Purtov KV, Petushkov VN, Baranov MS, Mineev KS, Rodionova NS, Kaskova ZM, Tsarkova AS, Petunin AI, Bondar VS, Rodicheva EK *et al*: **The Chemical Basis of Fungal Bioluminescence**. *Angew Chem Int Edit* 2015, **54**(28):8124-8128.

35. Oba Y, Suzuki Y, Martins GNR, Carvalho RP, Pereira TA, Waldenmaier HE, Kanie S, Naito M, Oliveira AG, Dorr FA *et al*: **Identification of hispidin as a bioluminescent active compound and its recycling biosynthesis in the luminous fungal fruiting body**. *Photochem Photobiol Sci* 2017, **16**(9):1435-1440.

36. Lee IK, Yun BS: **Highly oxygenated and unsaturated metabolites providing a diversity of hispidin class antioxidants in the medicinal mushrooms Inonotus and Phellinus**. *Bioorg Med Chem* 2007, **15**(10):3309-3314.

Tables

Table 1
NMR spectroscopic data of compound Aa)

position	*trans*-		*cis*-	
	δ_H	δ_C	δ_H	δ_C
2		173.9		173.5
3	*	90.0[b)]	*	*
4		168.0		168.1
5	6.11 s	102.1	6.13 s	104.0
6		162.2		162.1
7	6.60 d *J* = 16.0 Hz	117.1	5.98 d *J* = 12.8 Hz	119.0
8	7.31 d *J* = 16.0 Hz	137.4	6.72 d *J* = 12.8 Hz	139.2
9		129.0		128.8
10	7.03 d *J* = 2.0 Hz	115.0	6.98 d *J* = 2.0 Hz	117.2
11		147.0		146.3
12		148.8		147.8
13	6.77 d *J* = 8.0 Hz	116.7	6.73 d *J* = 8.0 Hz	116.3
14	6.95 dd *J* = 8.0, 2.0 Hz	122.1	6.80 dd *J* = 8.0, 2.0 Hz	123.4

a) Data (δ) were measured in CH_3OD at 400 MHz for protons and at 100 MHz for carbons. Proton coupling constants (*J*) in Hz are given in parentheses. The assignments were based on ^1H-^1H COSY, HSQC, and HMBC experiments.* Indicates the signal is not detected. *b*) Signals were extracted from HMBC spectrum.

Table 2
Quantity analysis of the DEPs

no.	Protein ID	Definition	Fold change			MRM fold change		
			32 h/control	128 h/32 h	128 h/control	32 h/control	128 h/32 h	128 h/control
1	GME472_g	hypothetical protein	2.66	2.25	5.18	7.02	2.25	15.80
2	GME555_g	HSP20 family protein	4.23	—	4.57	23.58	—	19.44
3	GME1626_g	F-type H+ -transporting ATPase	2.79	0.61	1.40	4.22	0.48	2.03
4	GME2462_g	hypothetical protein	3.33	—	3.64	5.36	—	6.64
5	GME3621_g	hypothetical protein	3.07	2.21	6.37	10.18	2.25	22.86
6	GME5465_g	F-type H+-transporting ATPase	3.32	0.64	1.90	3.62	0.36	—
7	GME6086_g	hypothetical protein	2.76	2.52	5.64	6.29	2.33	14.68
8	GME6848_g	GroES-like protein	1.98	1.81	3.50	3.15	2.38	7.50
9	GME8204_g	hypothetical protein	2.25	1.65	3.65	6.91	1.80	12.41
10	GME8292_g	GroES-like protein	2.20	2.82	5.99	5.66	3.51	19.85
11	GME10204_g	hypothetical protein	1.70	1.77	3.08	1.24	3.19	3.94

Table 3 The DEPs related to the biosynthesis of hispidin.

no.	Protein ID	Definition	Fold change		
			32 h/control	128 h/32h	128 h/control
1	GME4094_g	ketoacyl-synt-domain-containing protein	0.64	—	—
2	GME417_g	phenol 2-monooxygenase	—	—	1.52
3	GME418_g	hypothetical protein	2.06	—	2.67
4	GME10220_g	hypothetical protein	1.69	—	2.73
5	GME10204_g	hypothetical protein	1.7	1.77	3.08
6	GME7557_g	3-oxoacyl-[acyl-carrier protein] reductase	1.71	0.64	—
7	GME1172_g	NADH dehydrogenase (ubiquinone)	3.57	—	—
8	GME2933_g	NADH dehydrogenase (ubiquinone)	2.17	0.51	—
9	GME4242_g	Aldo/keto reductase family proteins	1.62	1.83	2.92
10	GME7978_g	2-oxoglutarate dehydrogenase	1.69	—	—
11	GME8093_g	NADH dehydrogenase (ubiquinone)	2.36	—	0.53
12	GME4762_g	NADH dehydrogenase	—	0.6	—
13	GME6232_g	NADH dehydrogenase	2.2	0.48	—
14	GME1172_g	NADH dehydrogenase	3.57	0.57	—
15	GME316_g	NADH dehydrogenase (ubiquinone)	2.31	—	—
16	GME4762_g	NADH dehydrogenase	—	0.6	—
17	GME6848_g	GroES-like protein	1.98	1.81	3.5
18	GME8093_g	NADH dehydrogenase (ubiquinone)	2.36	0.53	—
19	GME4242_g	Aldo/keto reductase family proteins	1.62	1.83	2.92
20	GME2933_g	NADH dehydrogenase (ubiquinone)	2.17	0.51	—

Table 4 The DEPs related to the biosynthesis of phelligridins.

no.	Protein ID	Definition	Fold change		
			32 h/control	128 h/32h	128 h/control
1	GME1855_g	ester dehydrase-isomerase	1.65	—	—
2	GME9431_g	acetate-hydrolyzing esterase	—	1.7	2.01
3	GME3566_g	carnitine *O*-acetyltransferase	—	1.53	1.53
4	GME2222_g	gibberellin 2-oxidase	—	1.55	—
5	GME1247_g	NADPH oxidase	—	1.57	—
6	GME4242_g	2-dehydropantolactone reductase	1.62	1.83	2.92
7	GME1010_g	aldo/keto reductase family proteins	—	1.65	—
8	GME4316_g	$NADPH_2$ dehydrogenase	—	3.79	4.22
9	GME1973_g	sulfonate dioxygenase	1.64	1.57	—
10	GME202_g	NADH-ubiquinone oxidoreductase	—	1.81	—
11	GME7140_g	predicted NAD-dependent oxidoreductase	3.8	2.59	—
12	GME272_g	norsolorinic acid ketoreductase	—	2.91	3.05
13	GME4319_g	NADH:flavin oxidoreductase	—	1.79	2.69
14	GME4553_g	alkylphenol/PAH-inducible cytochrome P450 monooxygenase	—	1.93	—
15	GME10364_g	norsolorinic acid ketoreductase	—	2.56	2.01
16	GME10320_g	oxidoreductase	2.08	—	2.02
17	GME10204_g	phenol 2-monooxygenase	1.7	—	3.08
18	GME11230_g	$NADPH_2$:quinone reductase	1.53	1.62	2.59
19	GME111_g	aldo-keto reductase	—	—	1.68
20	GME6807_g	cytochrome P450 monooxygenase	—	—	1.86
21	GME9582_g	$NADPH_2$ dehydrogenase	—	—	1.56
22	GME10875_g	oxidoreductase	1.55	—	1.54
23	GME7140_g	predicted NAD-dependent oxidoreductase	—	2.59	3.8
24	GME9574_g	$NADPH_2$ dehydrogenase	—	—	1.59
25	GME10600_g	diacetyl reductase	—	2.02	2.04
26	GME10220_g	phenol 2-monooxygenase	1.69	—	1.69
27	GME7574_g	FAD-dependent monooxygenase	—	—	1.61
28	GME2709_g	$NADPH_2$ dehydrogenase	—	—	1.84
29	GME10364_g	norsolorinic acid ketoreductase	—	2.56	2.01
30	GME606_g	$NADPH_2$:quinone reductase	—	3.49	2.91
31	GME4315_g	$NADPH_2$:quinone reductase	—	1.75	2.17
32	GME1966_g	Aldehyde dehydrogenase	—	—	1.58

33	GME2610_g	FAD-linked oxidoreductase	1.56	—	1.52
34	GME10317_g	monooxygenase	1.74	1.8	3.08

Figures

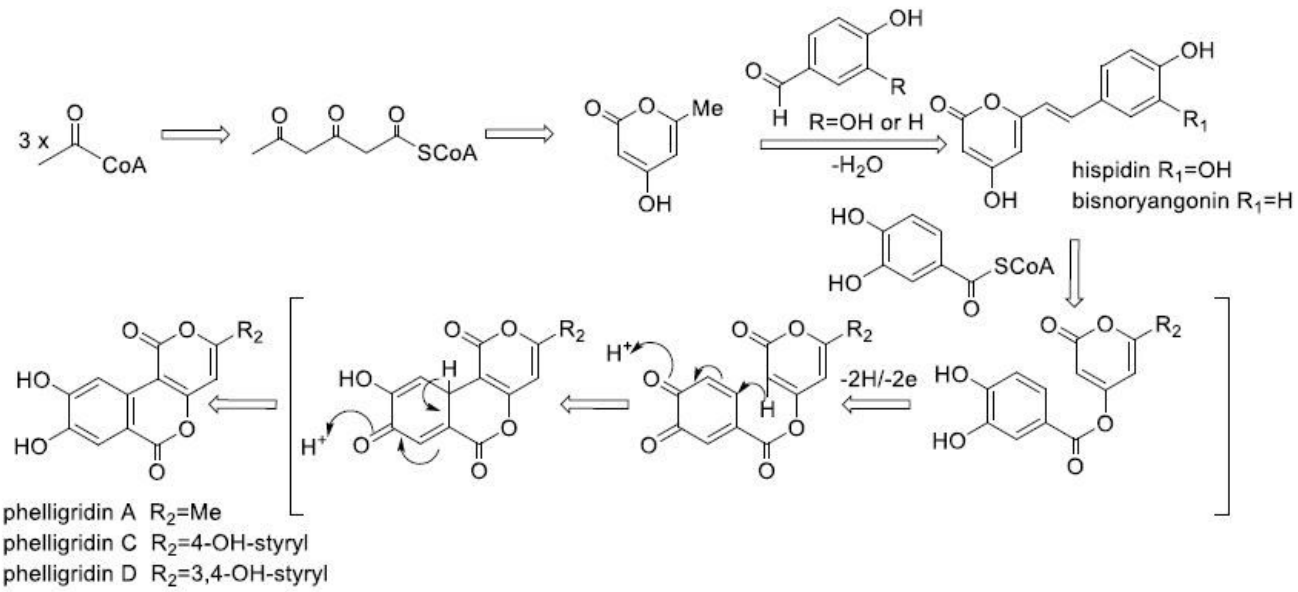

Figure 1

Figure 1

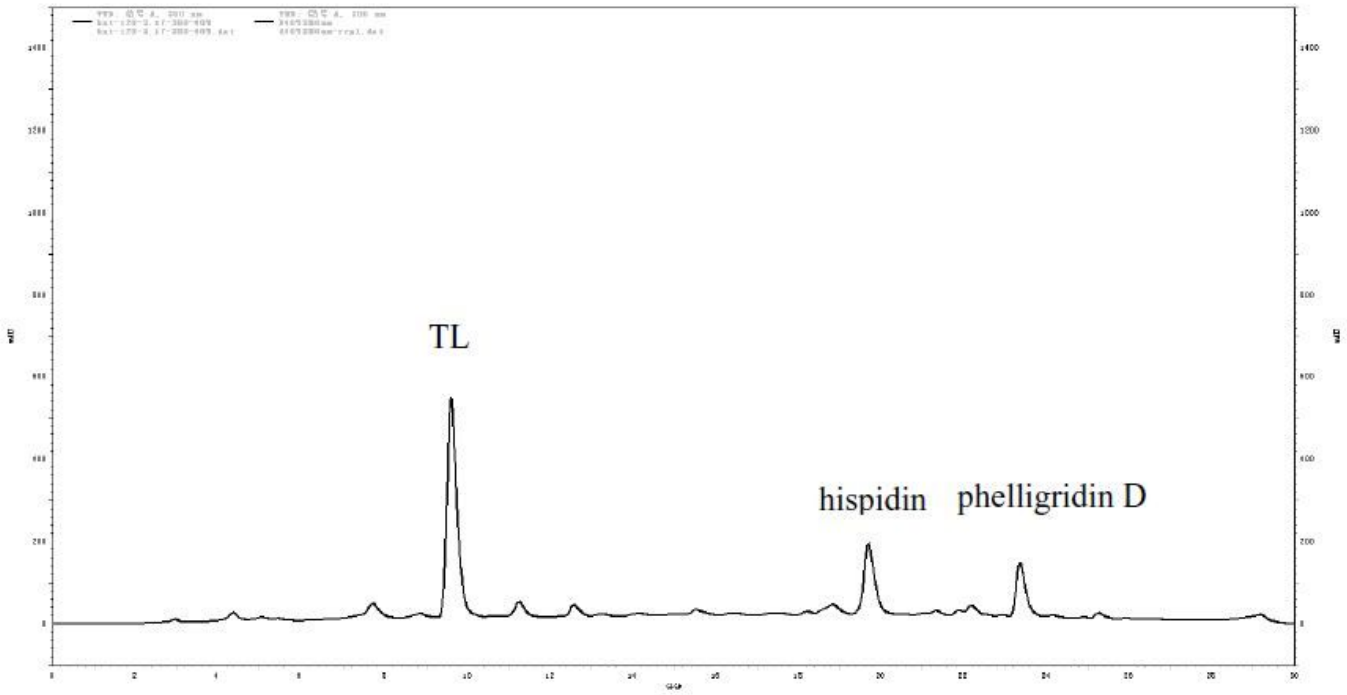

Figure 2

Figure 2

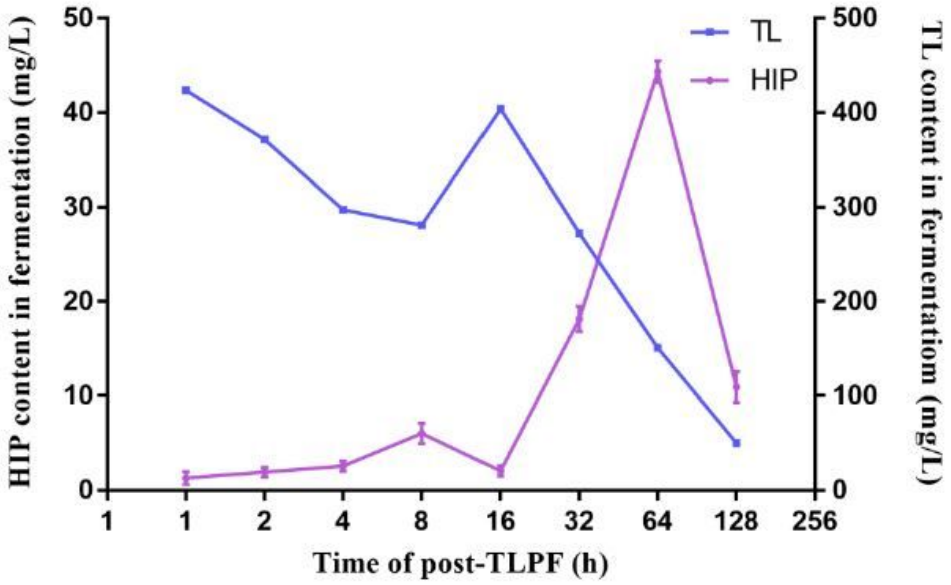

Figure 3

Figure 3

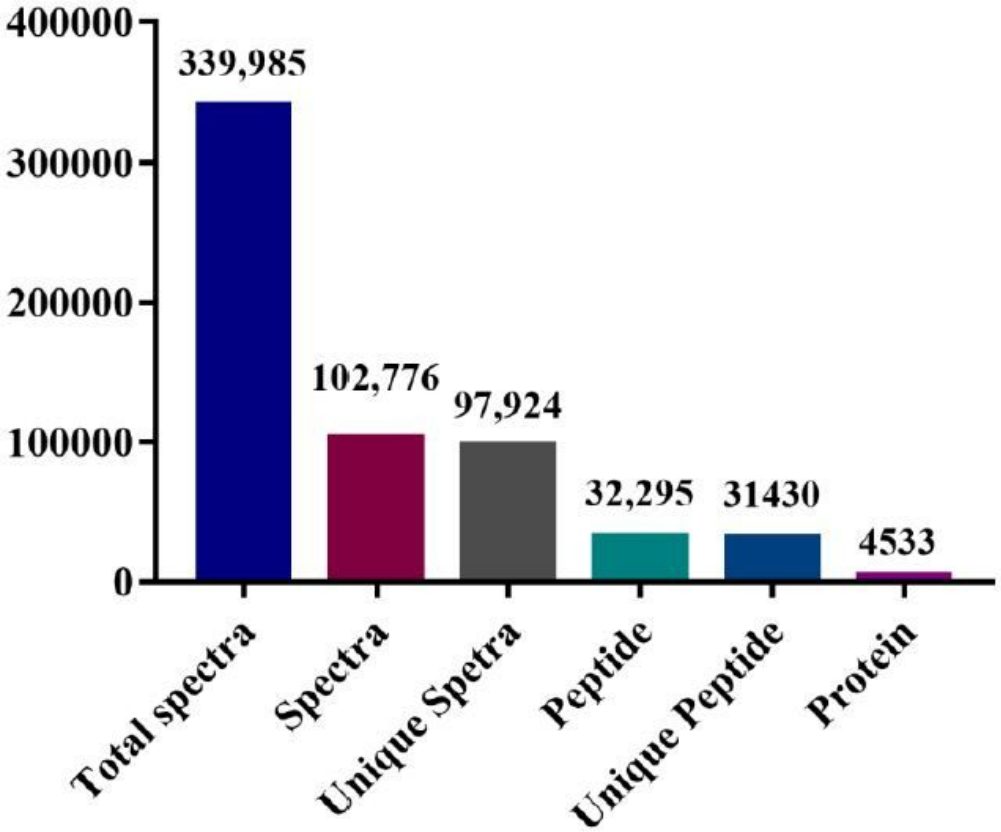

Figure 4

Figure 4

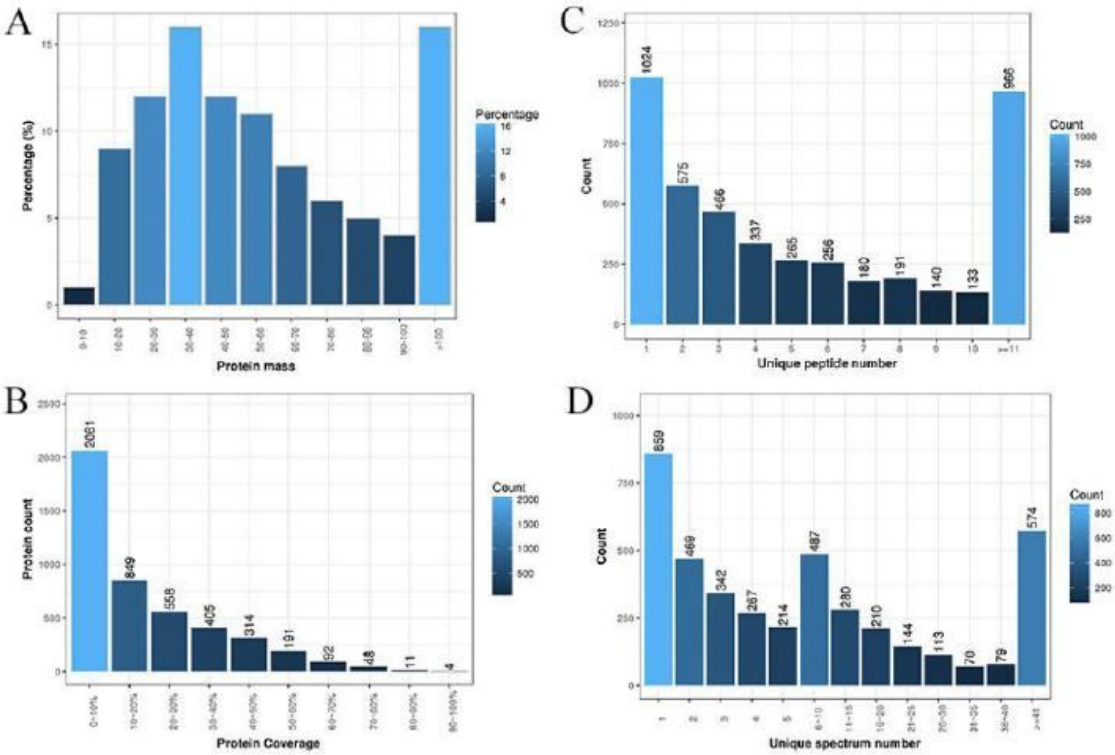

Figure 5

Figure 5

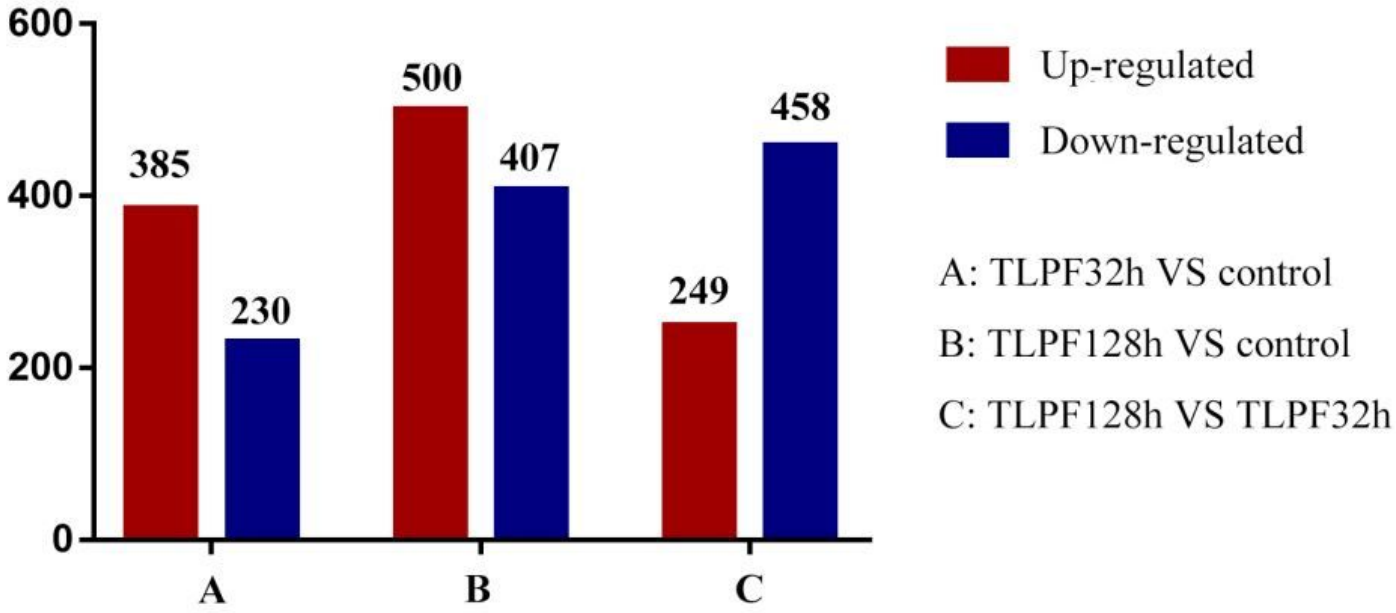

Figure 6

Figure 6

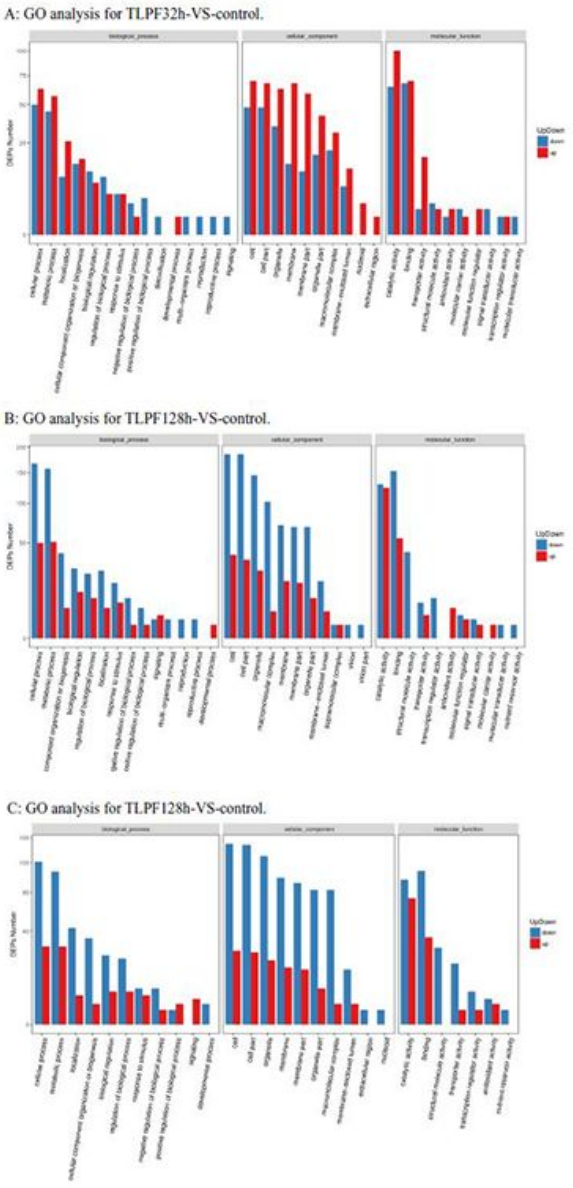

Figure 7

Figure 7

A: the KEGG pathway analysis for TLPF32h-VS-control.

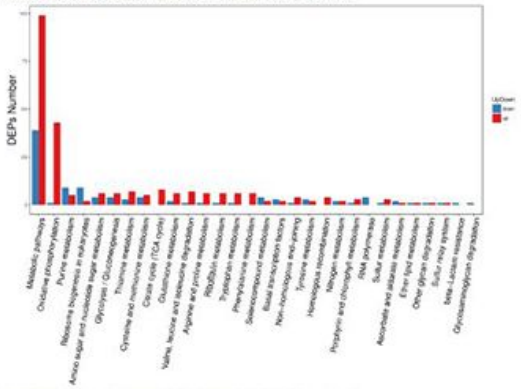

B: the KEGG pathway analysis for TLPF128h- VS-control.

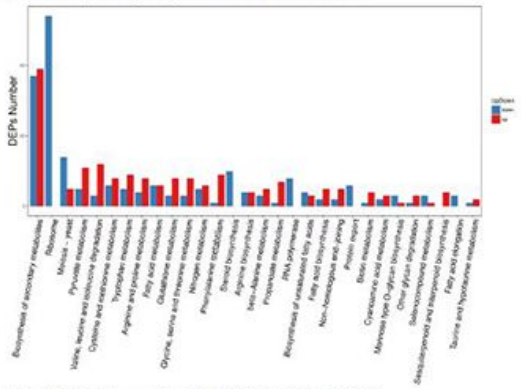

C: the KEGG pathway analysis for TLPF128h-VS- TLPF32 h.

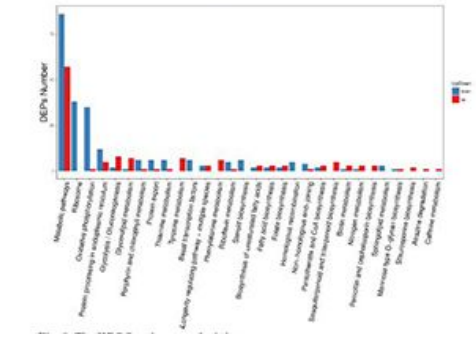

Figure 8

Figure 8

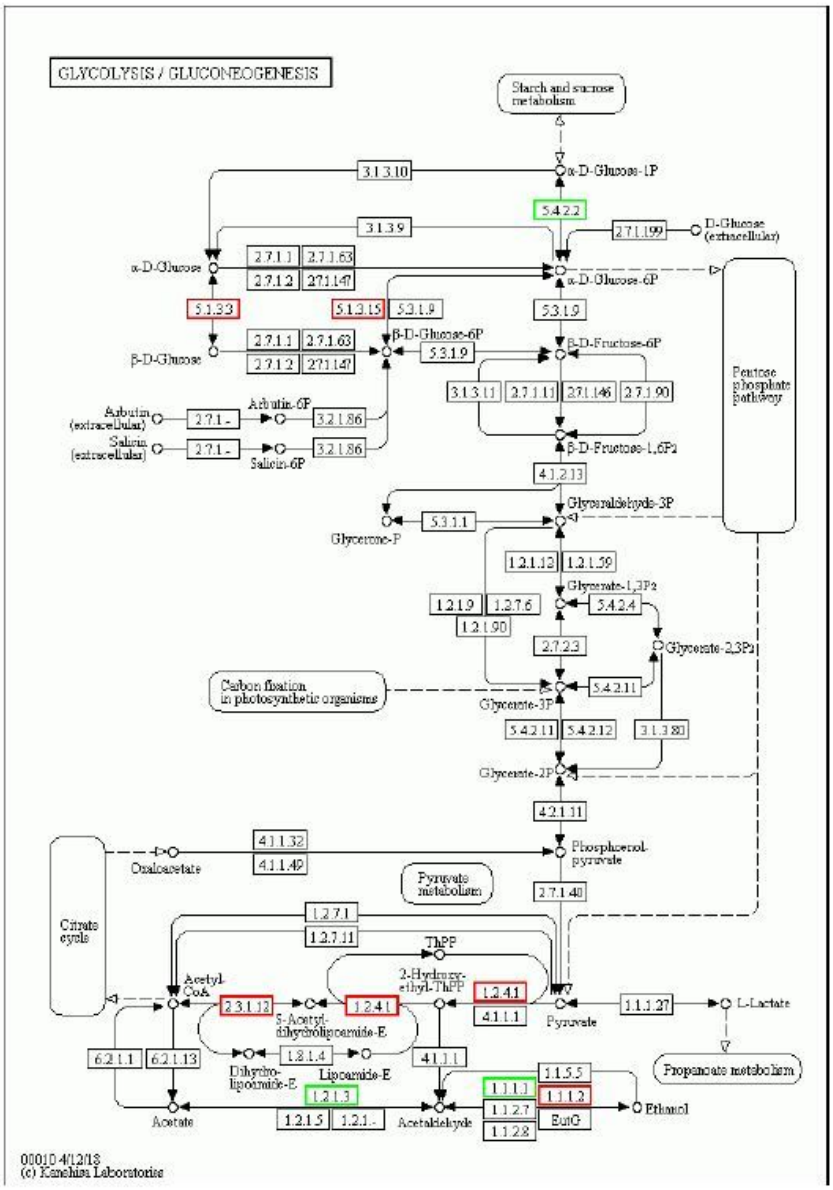

Figure 9

Figure 9

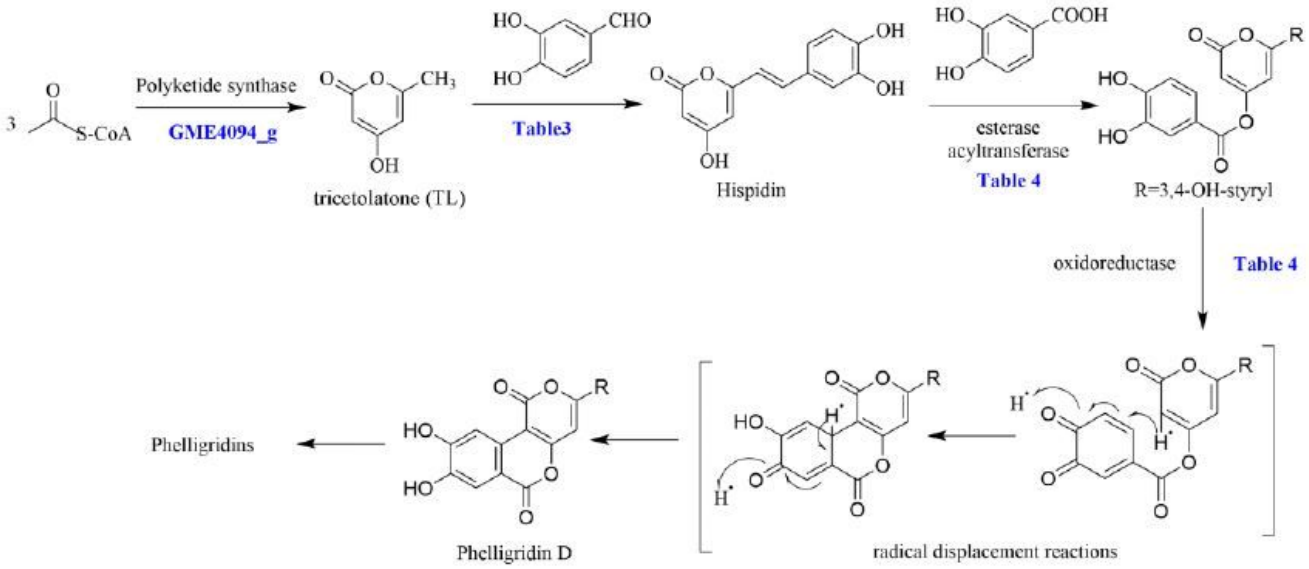

Figure 10

Figure 10